Heavy carrier effective masses in the van der Waals semiconductor Sn(SeS) revealed by high magnetic fields up to 150 T

Zhuo Yang,[1,*] Xueting Wang,[2] James Felton,[3] Zakhar Kudrynskyi,[3] Masaki Gen,[1] Toshihiro Nomura,[1] Xinjiang Wang,[2] Laurence Eaves,[3] Zakhar D. Kovalyuk,[4] Yoshimitsu Kohama,[1] Lijun Zhang,[2,†] and Amalia Patanè[3,‡]

[1] *Institute for Solid State Physics, The University of Tokyo, Kashiwa, Chiba, 277-8581, Japan*
[2] *Key Laboratory of Automobile Materials of MOE and College of Materials Science and Engineering, Jilin University, 2699 Qianjin Str., 130012, Changchun, China*
[3] *School of Physics and Astronomy, University of Nottingham, Nottingham NG7 2RD, UK*
[4] *Institute for Problems of Materials Science, The National Academy of Sciences of Ukraine, Chernivtsi Branch, Chernivtsi 58001, Ukraine*

(Dated: August 5, 2021)

The $SnSe_{2(1-x)}S_{2x}$ alloy is a van der Waals semiconductor with versatile, tunable electronic properties and prospects for future applications ranging from electronics to thermoelectrics and superconductivity. Its band structure and carrier effective masses underlie the quantum behaviour of charge carriers and hold great promise in future technologies. However, experimental measurement of these properties remains a challenging task. Here, magneto-transmission spectroscopy of $SnSe_{2(1-x)}S_{2x}$ thin films at pulsed magnetic fields B of up to 150 T reveals a large electron-hole reduced cyclotron mass $\mu^* > 0.454\ m_e$ (m_e is the free electron mass). This finding is supported by first-principle calculations of the band structure and by semiclassical Boltzmann transport theory, which predict a pronounced anisotropy of the carrier effective masses and electrical conductivity over two orthogonal directions (namely in the layer plane and out-of-plane) with a different anisotropy for electrons and holes. These properties are unique and important features of this class of compounds and are critical for understanding and using the tunable band structure of $SnSe_{2(1-x)}S_{2x}$ in fundamental and applied research.

I. INTRODUCTION

Tin disulphide (SnS_2), tin diselenide ($SnSe_2$) and the ternary alloy $SnSe_{2(1-x)}S_{2x}$ belong to the IV-VI group of layered van der Waals (vdW) crystals.[1, 2] They can be produced at low-cost, are environmentally friendly and have potential for applications in high performance thermoelectrics,[3, 4] electronics[5–7] and optoelectronics[8–10]. Although this class of vdW materials has been widely studied, some fundamental electronic properties, such as the carrier effective masses, are presently largely unknown. Carrier effective masses influence the electrical resistivity, optical absorption, thermalization of hot carriers *etc.* and hence affect the operation of electronic and optical devices. Thus, their measurement is essential to acquire better understanding of the $SnSe_{2(1-x)}S_{2x}$ alloy and to optimize its use in future applications.

$SnSe_{2(1-x)}S_{2x}$ is known to be an n-type semiconductor with a carrier concentration of up to 10^{17}-10^{18} cm^{-3}.[11–13] It has been used in high performance field effect transistors (FETs),[5] but its relatively low carrier mobility (up to 85 $cm^2V^{-1}s^{-1}$ at room temperature) represents a bottleneck for electronic device applications[5, 13–16]. In a simple Drude conductivity model, the carrier mobility is described by $\mu = e\tau/m^*$, where τ is the average scattering time, e is the elementary charge and m^* is the carrier effective mass.[17] Thus, a low mobility for charge carriers may result from a short scattering time τ due to elastic and inelastic collisions, and/or heavy carrier effective masses m^*, whose values are not yet known for the $SnSe_{2(1-x)}S_{2x}$ alloy. Theoretical works in the literature report large effective masses for holes: the valence band (VB) edge is located between the Γ and K points in the first Brillouin zone (FBZ) and exhibits a flat energy dispersion, corresponding to $m_h^* \geq 2m_e$.[18–21] However, there is large discrepancy in the literature regarding the value of the electron effective mass, which ranges from $m_e^* = 0.26\ m_e$ to $0.46\ m_e$. Also, the location of the conduction band (CB) edge in the FBZ is still debated.[19–21]

In this work, we report a magneto-transmission study of $SnSe_{2(1-x)}S_{2x}$ at high pulsed magnetic fields B of up to 150 T. A strong magnetic field can quantize the electron and hole motions into Landau level (LL) states, thus increasing the band gap energy of the semiconductor by $\hbar\omega_c^r/2$, where $\omega_c^r = eB/\mu^*$ is the cyclotron frequency and μ^* is the electron-hole reduced cyclotron mass. By measuring the energy of the absorption edge at high magnetic fields B of up to 150 T, we determine a lower limit for μ^* ($> 0.454\ m_e$). This estimate is supported by first-principle calculations of the electronic band structure of SnS_2 and $SnSe_2$, and by semiclassical Boltzmann transport theory of the conductivity effective masses for electrons and holes, indicating that these values have been underestimated in previous theoretical studies.[19–21] Furthermore, our work reveals that the carrier effective masses take distinct values along different crystallographic directions (namely in the layer plane and out-of-

* zhuo.yang@issp.u-tokyo.ac.jp
† lijun_zhang@jlu.edu.cn
‡ Amalia.Patane@nottingham.ac.uk

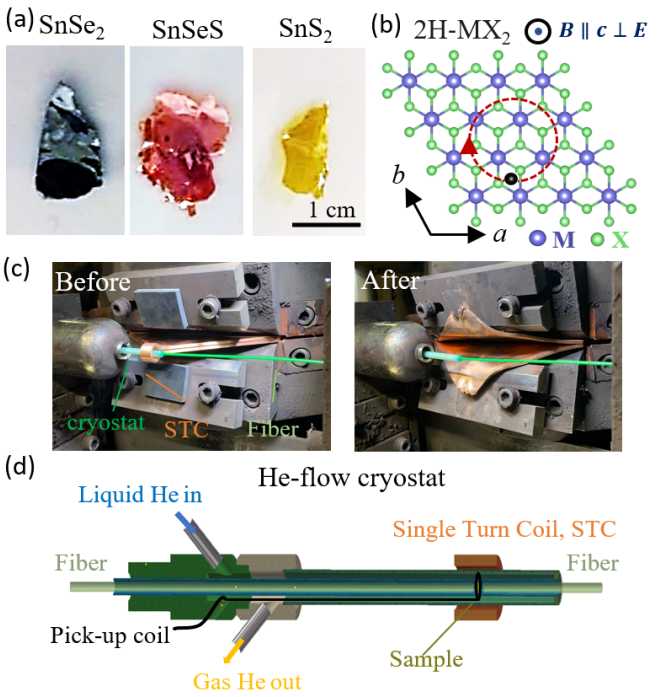

Figure 1. (a) Optical images of CVT-grown $SnSe_{2(1-x)}S_{2x}$. (b) Crystal structure for MX_2 (M = Sn and X = Se, S) and the orientation of magnetic field **B** relative to the a, b and c axis in the Faraday configuration. The red dashed line shows the semiclassical cyclotron motion of the electron in the ab plane. (c) Photos of single turn coil setup before and after the magneto-transmission measurements. (d) Schematic view of a specially-designed liquid-He flow-type cryostat for magneto-transmission measurements.

plane) and that this anisotropy is different for electrons and holes. The observation of these electronic properties provides a foundation for further investigations.

II. METHODS

$SnSe_{2(1-x)}S_{2x}$ ($0 \leq x \leq 1$) single crystals were grown by a chemical vapour transport (CVT) reaction method in a quartz ampoule using stoichiometric concentrations of high purity ($\geq 99.999\,\%$) reactants (Sn, S and Se) and iodine I_2 as the transport agent. The ampoule was kept in a furnace with a temperature gradient from T= 650 °C to T= 500 °C over a length of ∼10 cm: the reactants are introduced in the hot-region of the furnace tube and they crystallize in the cooler region over a period of 24 hours. As shown in Fig. 1(a), the as-grown crystals have the shape of flat platelets with mirror-like surfaces and in-plane areas of up to $\sim 1\ cm^2$. They have thickness L of up to ∼100 µm and can be readily exfoliated mechanically into nanometre-thick layers with a uniform composition x that can be adjusted over a wide range by changing the growth conditions.[22] For the polytype phase 2H - MX_2 (metal M = Sn; and chalcogen X = S, Se), the hexagonal unit cell consists of two weakly coupled vdW layers along the c-axis and strong covalent metal-chalcogen bonds within each layer (Fig. 1(b)).

For the magneto-optical transmission experiments on the $SnSe_{2(1-x)}S_{2x}$ alloys, a single-turn coil (STC) technique was employed to generate pulsed destructive magnetic fields of up to B = 150 T with typical pulse duration of 8 µs. During the pulsed magnetic field generation process, the single turn coil is destroyed by the strong electromagnetic force, as shown in Fig. 1(c). To obtain a measurable transmission signal, the thickness of the measured samples was reduced to ∼ 1 µm by mechanical exfoliation of the $SnSe_{2(1-x)}S_{2x}$ single crystals. The samples were placed in a specially-designed liquid-He flow-type cryostat, where the temperature can be controlled from 5 K to room temperature (see Fig. 1(d)).[23] The temperature of the sample was monitored by a type-E thermocouple (Nickel-Chromium/Constantan) and the value of the magnetic field was measured by a calibrated pick-up coil wound close to the sample. A Xenon arc-flash lamp was used as the light source. The light was guided and collected by 800 µm diameter optical fibres. The geometry of the single-turn pulsed magnetic field experiments with B up to 150 T is restricted to the Faraday configuration with **B**⊥**E** (the applied magnetic field **B** is perpendicular to the optical electric field **E** and to the ab layer plane of the crystal, as illustrated in Fig. 1(b)). The time-dependence of the transmitted light was measured by a high-speed streak camera coupled with a polychromator. For experiments in the Voigt configuration with **B**∥**E**, we used a non-destructive pulsed magnet field of up to B = 60 T with typical pulse duration of 36 ms. The sample was placed in an optical probe equipped with two 400 µm diameter optical fibres and two prisms. A broad band halogen lamp was used as the light source and the output signal was guided to a spectrometer equipped with a charge-coupled device (CCD) camera.

First-principles calculations were performed by density functional theory (DFT) using a plane-wave pseudopotential method, as implemented in the Vienna ab initio simulation package.[24, 25] The electron-ion interaction was described by means of projector-augmented wave pseudopotentials with Sn $5s^2 5p^2$, S $3s^2 3p^4$ and Se $4s^2 4p^4$ as the valence electrons. The exchange-correlation functional was treated by the generalized gradient approximation within the Perdew-Burke-Ernzerhof (PBE) formulation.[26, 27] The plane-wave cut-off energy was taken as 364 eV and a k-point grid spacing of $2\pi \times 0.04\ Å^{-1}$ was used for electronic Brillouin zone integration. For structural optimization, both atomic positions and cell parameters were relaxed until the residual forces of atoms were less than 0.05 eV/Å. To properly treat the dispersive vdW interaction in our system, the optB86b-vdW functional was adopted,[28, 29] which gives a satisfactory description of the binary Sn-S systems.[10, 30] Since the standard DFT-PBE methods suffer from problems which arise from under-estimation of the band gap due to spurious self-interaction, we em-

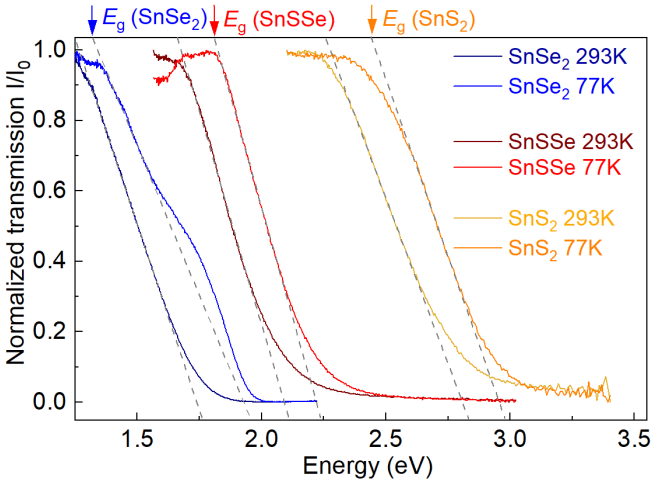

Figure 2. Normalized transmission spectra measured at T = 293 K and 77 K for thin films of $SnSe_2$, $SnSe_{2(1-x)}S_{2x}$ (nominal composition x = 0.5) and SnS_2. The absorption edge energies of the three samples at T = 77 K are marked with arrows. Dashed lines are guide to the eye.

ployed the Heyd-Scuseria-Ernzerhof (HSE06)[31] hybrid functional to give a more accurate description of the electronic band structures and thus of the band-edge second derivative carrier effective masses. The averaged carrier conductivity effective masses at 300 K were obtained using the semiclassical Boltzmann transport theory using the BoltzTraP code.[32] This takes into account the effects of non-parabolicity and anisotropy of the energy bands, and their degeneracy. Different electron (n) and hole (p) concentrations from 1.0×10^{15} to 1.0×10^{20} cm^{-3} were used for such calculations. The band energy isosurfaces were calculated by the method of Wannier interpolation based on the use of a unique set of Wannier functions[33] and were visualized through the FermiSurfer code.[34]

III. RESULTS AND DISCUSSION

Fig. 2 shows the normalized transmission spectra (I/I_0) measured at 293 K and 77 K for films of $SnSe_2$ (thickness t = 1.4 µm, see Sec. I in the Supplemental Material [35] and references [36, 37] therein) and SnS_2 (t = 0.6 µm, see Sec. I in the Supplemental Material [35] and references [38, 39] therein) together with the spectrum of the ternary alloy $SnSe_{2(1-x)}S_{2x}$ (nominal composition x = 0.5). Here, I_0 is the intensity of the light transmitted through the system in the absence of the layers. The spectra reveal clearly the large blue shift of the absorption edge with increasing S-content and with decreasing temperature, consistent with previous measurements.[40] For all three layers the spread in energy across the transmission edge is large, ∼0.3 eV (see grey dashed line in Fig. 2), consistent with the indirect band gap nature of these van der Waals semiconductors.[22, 40] We observe no clear evidence of an excitonic absorption feature even at low temperatures. The composition of the alloy can be adjusted over a wide range, indicating good miscibility of the SnS_2 and $SnSe_2$ compounds. The composition-dependence of the indirect bandgap energy E_g corresponds to a large bowing coefficient $b \approx 1$ eV, arising from volume deformation and charge exchange effects due to the different sizes and orbital energies of the S- and Se-atoms. This also causes a composition-dependence of the phonon energy modes, electron–phonon interaction, and temperature dependence of E_g.[22]

Fig. 3 shows the low temperature (T = 10 K) magneto-transmission spectra of SnS_2 and $SnSe_{2(1-x)}S_{2x}$ (nominal composition x = 0.5) with magnetic field B of up to 150 T in the Faraday configuration. We focus on the magneto-transmission data in Fig. 3 and Sec. III in the Supplemental Material [35] at low temperature (T = 10 K) to avoid thermal broadening of the Landau levels. The time dependence of the magnetic field pulse is shown in Fig. 3(a), (d). Fig. 3(b), (e) are the streak camera images of the transmission. Here, the normalized transmission, I/I_0, is represented by a colour scale. During the pulsed field measurement, the streak camera is synchronized with the magnetic field pulse. Therefore, the streak image in Fig. 3(b), (e) shows the dependence of the transmission spectrum on B. To compare the spectra measured from zero magnetic field to the maximum field, we extract the transmission spectra at 0 T, 50 T, 100 T and 150 T from the cross-section of the streak camera image (see the color markers in Fig. 3(b),(e)), and plot them on the same frame, as shown in Fig. 3(c),(f). The data show that a magnetic field of 150 T has no observable effect on the transmission spectra. Similar results were obtained in the Voigt configuration (see Sec. II in the Supplemental Material [35]). Also, the $SnSe_2$ samples were measured under the same conditions described above for SnS_2 and $SnSe_{2(1-x)}S_{2x}$ (nominal composition x = 0.5), and for all samples, no measurable changes were observed in high magnetic fields (see Sec. III in the Supplemental Material [35]).

Magnetic fields are often used to probe fundamental properties of semiconductors. However, for $SnSe_{2(1-x)}S_{2x}$, even magnetic fields as high as 150 T cannot reveal any change of the transmission spectrum. The absence of a measurable effect at such large magnetic fields (up to 150 T) for a bulk semiconductor is surprising and rarely observed. At first glance, this may raise questions about the reliability of the data and experimental setup. To rule out these possibilities, we also performed magneto-transmission studies of the well-known vdW semiconductor InSe under the same conditions used for $SnSe_{2(1-x)}S_{2x}$. As shown in the Sec. IV of the Supplemental Material [35] (see, also, references [41–45] therein), the magnetic field dependence for InSe samples agree well with the previous magneto-optical study of InSe by Millot et al., revealing Landau level quantization at high B.[43, 44] The shift of the absorption edge for InSe in a magnetic field is due to the diamagnetic

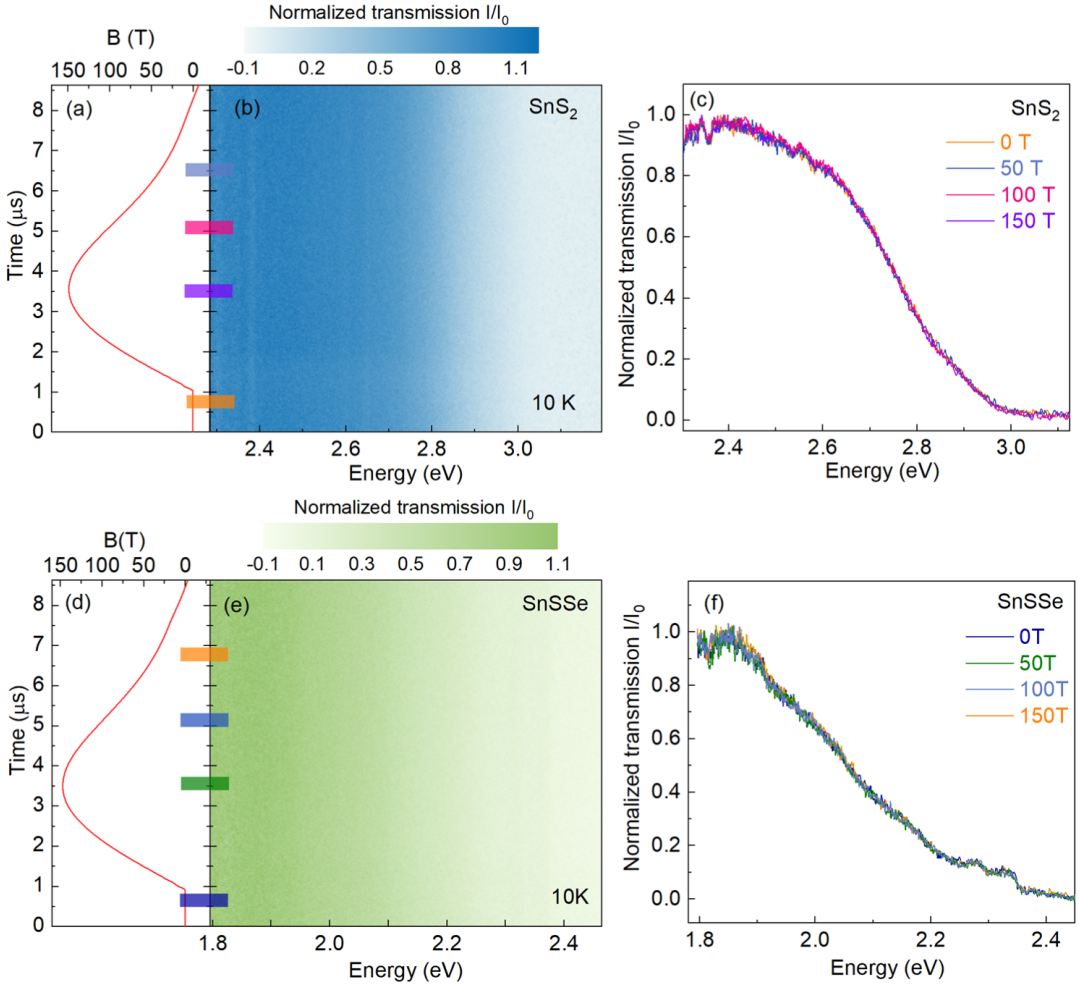

Figure 3. (a), (d) Time dependence of the magnetic field B pulse with values sweeping from $B = 0\,\mathrm{T}$ to $B = 150\,\mathrm{T}$. (b), (e) Streak camera image of the optical transmission of SnS_2 and $SnSe_{2(1-x)}S_{2x}$ (nominal composition x = 0.5) at 10 K with magnetic field of up to $B = 150\,\mathrm{T}$. Color markers indicate the cross-section positions in the streak camera image at $B = 0\,\mathrm{T}$, 50 T, 100 T and 150 T. (c), (f) Normalized transmission spectra at indicated magnetic field ($T = 10\,\mathrm{K}$).

shift of an exciton state. At low B ($< 30\,\mathrm{T}$), this is well decribed by a quadratic dependence.[44] However, for a cyclotron energy $\hbar\omega_c$ larger than the exciton binding energy, the shift in magnetic field increases linearly with B, fully consistent with the shift of the $N = 0$ Landau level ($\hbar\omega_c/2$).[23] Finally, we point out that our set up has been used previously to measure different systems, including: GaAs/AlGaAs superlattices,[46] GaSe[47] and 2D halide perovskites.[48]

To interpret our findings, we consider the behaviour of indirect band gap semiconductors in magnetic field. For an indirect band gap semiconductor such as the $SnSe_{2(1-x)}S_{2x}$ alloy, the dependence of the band-edge absorption energy on magnetic field can be expressed as[49, 50]

$$E(B) = E_g \pm \hbar\omega_0 + (N + \frac{1}{2})\hbar\omega_c^h + (N' + \frac{1}{2})\hbar\omega_c^e, \quad (1)$$

where E_g is the indirect band gap energy, $\hbar\omega_c^{e/h}$ is the cyclotron energy of carriers, $\omega_c^{e/h} = eB/m_{e/h}^*$, and $m_{e/h}^*$ is the cyclotron mass for electrons/holes. Here, N and N' are the Landau level quantum numbers for electrons and holes, respectively. Indirect gap optical transitions are assisted by the emission or absorption of phonons of energy $\hbar\omega_0$. The sign $\pm$ in Eqn. 1 refers to the absorption (+) or emission (−) of the phonon energy in the optical transition. As shown in Fig. 3(c)(f) and Sec. III in the Supplemental Material [35], the measured transmission reveals a clear absorption edge. However, no Landau quantization is observed and the absorption edge energy does not change with increasing B.

In the magneto-absorption spectra of a semiconductor, the Landau level transitions may become unresolved due to energy broadening effects caused by disorder. However, our transport measurements on $SnSe_2$ shows a quadratic magnetoresistance at relatively low applied magnetic fields ($B \sim 5\,\mathrm{T}$) (see Sec. VI in the Sup-

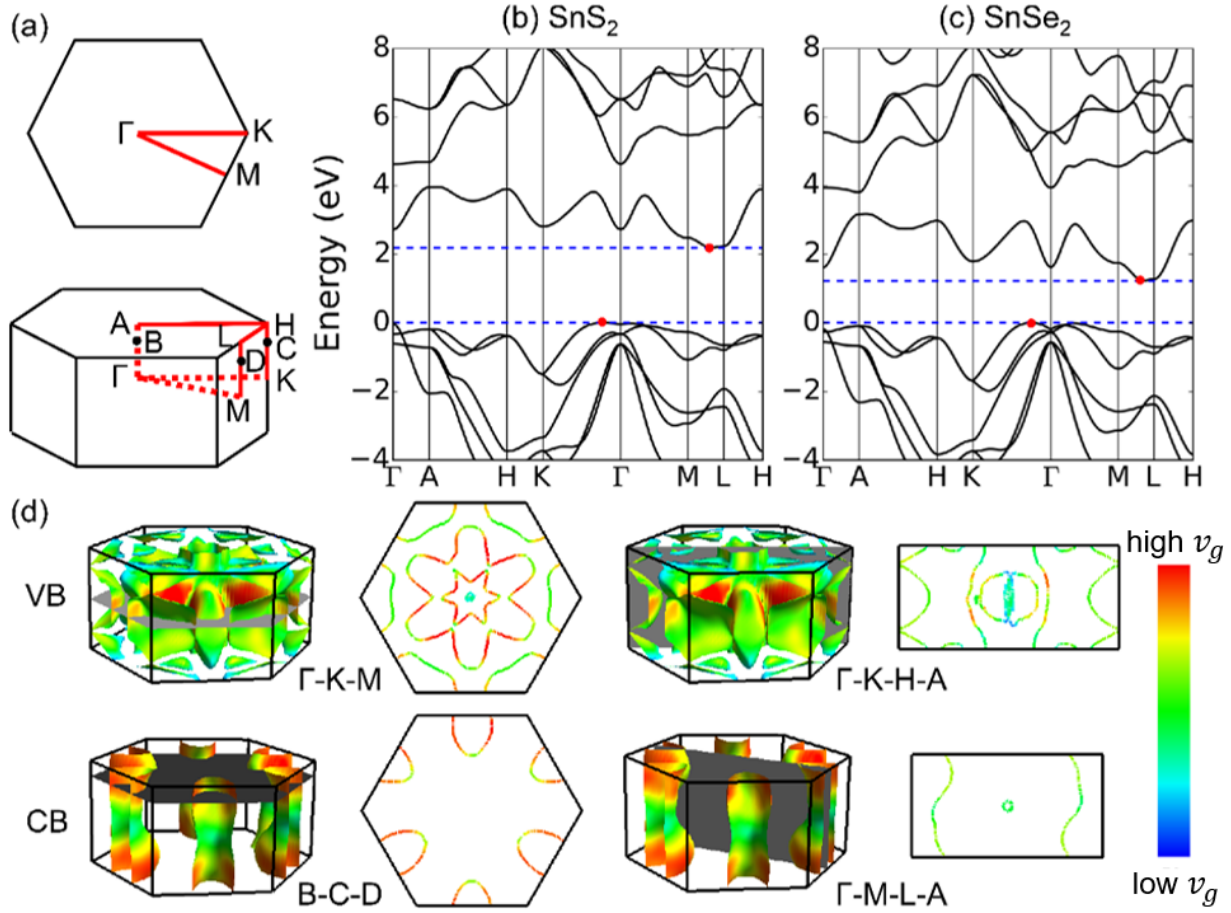

Figure 4. (a) Schematics of two-dimensional (top) and three-dimensional (bottom) Brillouin zones. (b)-(c) The calculated band structure of SnS_2 and $SnSe_2$. The valence band maximum (VBM) is set to zero energy. The red dots indicate the conduction band (CB) and VB edges. (d) Three-dimensional band energy isosurfaces and cross sections containing the band-edge k-points of SnS_2 highlighting several hole and electron pockets. The band energy isosurfaces correspond to an energy of 0.69 eV below the VBM and 0.55 eV above the CB minimum (CBM). (D) is the k-point of the CBM and B-C-D plane is parallel to the -K-M plane: B (0.00, 0.00, 0.33), C (-0.33, 0.67, 0.33), D (0.00, 0.50, 0.33). The colour bar corresponds to the group velocity v_g from low (blue) to high (red) values.

plemental Material [35] and references [51, 52] therein), which would not be expected in a highly disordered system.[51, 52] Therefore, we exclude the possibility that our findings arise from a broadening of LLs caused by disorder. Furthermore, we note that our magneto-transmission spectra do not reveal any broadening or narrowing of the absorption edge with increasing B. This would be expected due to the magnetic-field quantization of the electron motion: as B increases from $B = 1$ T to $B = 150$ T, the magnetic length, $l_B = \sqrt{(\hbar/eB)}$, decreases from $\sim$ 26 nm to 2 nm. At $B = 150$ T, l_B is less than an order of magnitude larger than the lattice constants of the $SnSe_{2(1-x)}S_{2x}$ alloy ($a = b = 0.36$ nm and $c = 0.59$ nm for SnS_2; $a = b = 0.38$ nm and $c = 0.61$ nm for $SnSe_2$).[22] For potential fluctuations on a large length scale ($> l_B$), a decrease of l_B would induce a narrowing of the absorption edge.[53] On the other hand, for potential fluctuations on a short length scale ($< l_B$), a decrease of l_B would broaden the absorption edge.[53] Neither of these scenarios are observed. In addition to the disorder, another possibility is that the cyclotron energy shift is cancelled by a simultaneous Zeeman shift. To measure the Zeeman shift, we have conducted the magneto-transmission experiments with left/right circularly polarized light (see Sec. V in the Supplemental Material [35]). However, no observable energy shift was observed. Thus, we exclude this possibility. Alternatively, the absence of a measurable change in the magneto-transmission under high magnetic fields can be assigned to intrinsic electronic properties. According to Eqn. 1, the shift of the band gap energy due to the magnetic field is $\Delta E \sim (\hbar\omega_c^h + \hbar\omega_c^e)/2$. Here we assume that the phonon energy $\hbar\omega_0$ does not change with B since the magnetic field does not induce any structural change of the $SnSe_{2(1-x)}S_{2x}$ alloy. Our data indicate no measurable energy shift at $B = 150$ T, suggesting a large reduced electron-hole cyclotron mass $\mu^* = m_h^* m_e^*/(m_h^* + m_e^*)$. To estimate its value, we should compare ΔE with the energy uncertainty ΔE_0 of the

measurement. Thus, we write

$$\Delta E = \frac{\hbar e B}{2\mu^*} \leq \Delta E_0. \quad (2)$$

Two methods were used to estimate ΔE_0 (see Sec. VII in the Supplemental Material [35] and reference [38] therein). The first method is based on the energy resolution of the measurement equipment, which yields ΔE_0 = 0.019 eV. As for the second method, we fitted the transmission data using a theoretical model for the transmission of an indirect band gap semiconductor. The fit uncertainty is estimated using an R-squared method to evaluate the scatter of the data points around the fitted line. This method gives ΔE_0 = 0.017 eV. Based on the two models above, we estimated that the lower limit for the cyclotron mass μ_L^* is 0.454 m_e (ΔE_0 = 0.019 eV) and 0.511 m_e (ΔE_0 = 0.017 eV), respectively. These two values correspond to reduced effective masses that are significantly heavier than those of most well-known semiconductors. Since μ^* is smaller than the individual cyclotron masses $m_{e/h}^*$, we infer that both the electron and hole cyclotron masses should be larger than 0.454 m_e. Gonzalez et al.[20] have calculated the band structure of $SnSe_2$ and SnS_2, indicating a reduced mass value of μ^* = 0.345 m_e and 0.365 m_e for $SnSe_2$ and SnS_2, respectively. If we assume these values, we should be able to observe a band edge energy shift of $\Delta E \sim 50$ meV at B = 150 T, which is well above the energy uncertainty ΔE_0. Thus, our data for SnS_2 and $SnSe_{2(1-x)}S_{2x}$ (x = 0.5) in Fig. 3 and those for $SnSe_2$ in the Supplemental Material [35] are strongly indicative of heavy carrier masses. As discussed below, these findings are supported by our first-principle density functional theory (DFT) of the electronic band structure (for details, see Methods section).

Fig. 4 shows the calculated electronic band structure for SnS_2 and $SnSe_2$. As can be seen in Fig. 4(b-c), both compounds have indirect band gaps (E_g): the values of E_g = 2.19 eV for SnS_2 and 1.23 eV for $SnSe_2$ are close to our measured values (E_g (SnS_2) = (2.14 ± 0.03) eV and E_g($SnSe_2$) = (1.20 ± 0.03) eV at 300 K.[22] For both compounds, the conduction band minimum (CBM) is located along the M-L line in the Brillouin zone; the valence band maximum (VBM) is instead along the line Γ-K, close to Γ, at about 30 % of the Γ-K wave-vector. This is consistent with angle-resolved photoemission spectroscopy measurements on $SnSe_2$, which indicate a VBM in proximity of the Γ-point.[14] Also, we note that in the vicinity of the VBM there is an additional lower energy band edge along the line Γ-M, leading to a VB that takes the form of an inverted, asymmetric "Mexican hat".

The CB and VB are both weakly dispersed and highly anisotropic. To illustrate the anisotropy more clearly, we show in Fig. 4(d) the three-dimensional band energy isosurfaces and the cross sections containing the band-edge k-points for SnS_2, as calculated using the method described in the Methods section. The band energy isosurfaces are plotted at an energy of 0.69 eV below the VBM (top panel of Fig. 4(d)) and 0.55 eV above the CBM (bottom panel of Fig. 4(d)). The conduction band is more dispersive in the plane than along the out-of-plane direction, resulting in a larger carrier group velocity and a lighter effective mass for conduction electrons in the layer plane. The behaviour for holes is opposite, with a lighter effective mass along the out-of-plane direction. Also, the valence band exhibits a complex structure with multiple degenerate, anisotropic bands near the valence band-edge. Similar findings apply to $SnSe_2$. The complex, anisotropic electronic band structure of these compounds requires a careful analysis of the carrier effective masses and their comparison with the experiment.

Table I shows the calculated band-edge second derivative effective masses for electrons (m_e^*) and holes (m_h^*) along the k_x, k_y, k_z directions of the Brillouin zone of SnS_2 and $SnSe_2$. Due to the anisotropic band structure, the band edge dispersion is non-parabolic, making it impossible to assign a single effective mass value for each k-direction. We calculate the hole effective mass from the energy dispersion along K-X and X-Γ near the VB edge. Similarly, we calculate the electron effective mass from the energy dispersion along M-Y and Y-L near the CB edge. Here, X and Y represent the band edge for the VB and CB, respectively. From Table I, it can be seen that the second derivative effective masses for electrons (m_e^*) and holes (m_h^*) take distinct values for each k-direction. Considering that optical measurements probe the energy levels near the band edge regardless of the k-direction, the anisotropic second derivative effective mass values cannot be used for a comparison with the experimental data.

Table I. Band-edge second derivative electron (m_e^*/m_e) and hole (m_h^*/m_e) effective masses in the k_x, k_y, k_z directions of the Brillouin zone and their geometric average ($\overline{m}^*/m_e$) for SnS_2 and $SnSe_2$. These are calculated using DFT.

Compound		m_h^*/m_e		m_e^*/m_e	
		K-X	X-Γ	M-Y	Y-L
SnS_2	k_x	8.973	6.150	7.547	6.233
	k_y	39.639	34.563	8.494	12.254
	k_z	9.706	9.685	65.460	98.711
	$\overline{m}^*/m_e$	12.515	10.177	11.300	11.897
$SnSe_2$	k_x	6.285	23.427	6.285	5.105
	k_y	7.257	4.735	7.257	10.811
	k_z	38.795	12.552	38.795	62.667
	$\overline{m}^*/m_e$	9.297	8.995	9.297	9.857

Alternatively, we use Boltzmann transport calculations applied to the calculated band structures to extract the conductivity effective mass for electron and hole motions along different crystallographic directions, in the layer plane (m_t^*) and out-of-plane (m_l^*), and their geometric average $\overline{m}^*$. In this model, we consider a range of carrier concentrations for electrons and holes (from 10^{15} to 10^{20} cm^{-3}). Table II shows the calculated conductivity effective masses for a non-degenerate semiconductor with a hole and electron density of 10^{15} cm^{-3}. These values change by less than 10 % with increasing the electron and

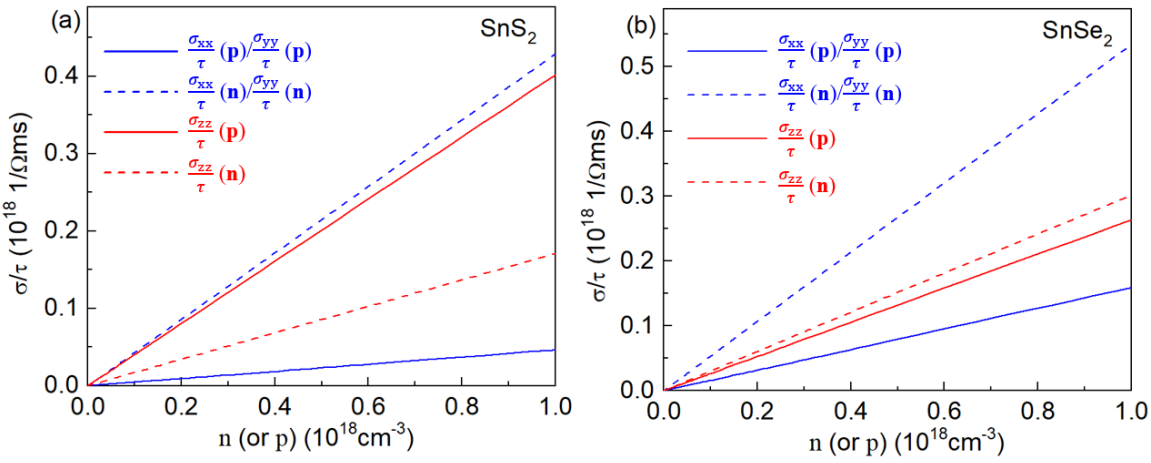

Figure 5. Calculated values of the ratio between the components of the conductivity tensor, σ_{xx}, σ_{yy}, and σ_{zz}, and the relaxation time τ versus the carrier concentration n (or p) for (a) SnS_2 and (b) $SnSe_2$ at 300 K. Solid and dashed lines refer to p-type and n-type transport, respectively.

hole density up to 10^{18} cm^{-3} (see Sec. VIII in the Supplemental Material [35]).

Table II. Conductivity effective masses in the plane (m_t^*) and out-of-plane (m_l^*) for electrons (m_e^*), holes (m_h^*), and electron-hole pairs (μ^*) in SnS_2 and $SnSe_2$, as calculated using the semiclassical Boltzmann transport theory at 300 K and a carrier density of 10^{15} cm^{-3}. The Cartesian directions are x along $\boldsymbol{a}$, y along $\boldsymbol{b}$, and z normal to x and y ($\boldsymbol{c}$-axis). The values for the geometric average of m_t^* and m_l^* ($\overline{m}^*/m_e$) and $\sqrt{m_l^* m_t^*}/m_e$ are also shown.

Compound		m_t^*/m_e		m_l^*/m_e	$\sqrt{m_t^* m_l^*}/m_e$	$\overline{m}^*/m_e$
		x	y	z		
SnS_2	m_h^*/m_e	4.124	4.124	0.481	1.408	1.169
	m_e^*/m_e	0.447	0.447	1.117	0.707	0.559
	μ^*/m_e	0.403	0.403	0.336	0.471	0.378
$SnSe_2$	m_h^*/m_e	1.101	1.101	0.649	0.845	0.893
	m_e^*/m_e	0.392	0.392	0.689	0.512	0.458
	μ^*/m_e	0.289	0.289	0.334	0.322	0.302

As shown in Table II, the geometric averaged conductivity effective mass for electrons and holes in SnS_2 is $\overline{m}^* = 1.169\ m_e$ and $0.559\ m_e$, respectively. The corresponding values in $SnSe_2$ are $\overline{m}^* = 0.893\ m_e$ and $0.458\ m_e$. These large carrier effective masses originate from the dispersionless nature of the band-edge states. This is rooted in the chemical bonding between the Sn and the chalcogen (S and Se) atoms within the particular crystalline symmetry associated with the 2D layered structure.[20, 54] The calculated electron masses (see Table I and II) are significantly larger than in other semiconductors, such as GaAs ($0.067\,m_e$),[55] hybrid organic-inorganic perovskites (0.09 to $0.14\,m_e$),[56–59] and several vdW semiconductors, such as $WSe_{2(1-x)}S_{2x}$ (0.15 to $0.21\,m_e$),[60, 61] SnSe (0.17 to $0.21\,m_e$)[62] and InSe ($0.138\,m_e$).[41, 44] These heavy carrier effective masses can account for the relatively low electron mobility reported in $SnSe_2$ and SnS_2 (<85 cm^{2}V^{-1}s^{-1} at room temperature),[5, 13–16] which is one or two orders of magnitude lower than in other vdW crystals, such as InSe[63] or traditional semiconductors, such as GaAs.[64]

We note that the conductivity effective masses in the plane (m_t^*) and out-of-plane (m_l^*) are significantly different (Table II): for holes, out-of-plane masses tend to be smaller than in the layer plane, particularly for SnS_2. In contrast, electron masses tend to be lighter in the layer plane than out-of-plane. The anisotropic energy dispersions of these compounds imply that careful consideration should be paid to the orientation of the applied magnetic field when assessing the cyclotron mass. In the Faraday configuration, the measured cyclotron mass reflects primarily the in-plane carrier masses (m_t^*). We find that the calculated in-plane electron-hole reduced mass for SnS_2 ($\mu^* = 0.403\,m_e$, Table II) is slightly lower than μ_L^* ($0.454\,m_e$ - $0.511\,m_e$) obtained experimentally. To probe the out-of-plane effective mass (m_l^*) in SnS_2, we measured the magneto-transmission spectra of SnS_2 in the Voigt configuration (see Sec. II in the Supplemental Material [35]). In the Voigt geometry and for an anisotropic material, the cyclotron mass is a square root average of the in-plane and out-of-plane masses ($\sqrt{m_l^* m_t^*}$).[65] The reduced electron-hole mass derived from the measurements for SnS_2 indicate $\mu^* > 0.4\,m_e$, which is consistent with the calculated value of $\mu^* = 0.471\,m_e$ (Table II). For $SnSe_2$, the calculated masses are lighter than for SnS_2 and smaller than μ_L^* ($0.454\,m_e$ - $0.511\,m_e$) suggested by the experiment. This discrepancy may arise from the contribution of the electron-phonon interaction, which is important in these compounds due to the strong Sn- S and Sn-Se covalent bonding and charge localization around the S- and Se-atoms.[22] The contribution of the electron-phonon interaction to the effective mass was not considered here and requires further investigation. This interaction can distort energy dispersions leading to the mass renormalization.

Our findings on the anisotropic band structure and large effective masses underlie important functionalities of $SnSe_{2(1-x)}S_{2x}$, including its transport properties. Fig. 5(a) and (b) show the calculated dependence of the ratio between the components of the conductivity tensor σ_{xx}, σ_{yy}, and σ_{zz}, and the relaxation time τ, versus the carrier concentration for SnS_2 and $SnSe_2$, respectively. To calculate the conductivity, we have used the semiclassical Boltzmann transport theory and the simplifying assumption of a constant relaxation time τ. From Fig. 5, it can be seen that for all directions the conductivity varies almost linearly with the electron (n) and hole (p) density. This is expected from a simple Drude model in which the conductivity increases linearly with the carrier density. Furthermore, within the range of n and p considered here (up to 10^{18} cm^{-3}), the carrier mobility remains approximatively constant due to a weak dependence of the carrier effective mass on n and p. For both SnS_2 and $SnSe_2$, n-type conductivity is more favourable along the x and y directions than along the z-direction. Thus, the electron current is expected to flow more easily in the layer plane than from one layer to the adjacent one. The behaviour of holes is qualitatively different: p-type transport is more favourable along the z-direction. Such anisotropy arises from anisotropic band structures and distinct anisotropic properties for electrons and holes. It indicates that $SnSe_{2(1-x)}S_{2x}$ is a semiconductor with a quasi-1D character for holes and quasi-2D character for electrons.

IV. CONCLUSIONS

In conclusion, we have shown that the magneto-optical transmission spectrum of the $SnSe_{2(1-x)}S_{2x}$ compound does not show a statistically significant change with applied magnetic fields of up to 150 T. This observation indicates that hole and electron effective masses are large, in good agreement with first-principle band structure calculations and semiclassical Boltzmann transport theory. The dispersionless nature of the band-edge states originate from the chemical bonding between the Sn and the chalcogen (Se and S) atoms within the crystalline symmetry associated with the polytype phase 2H-MX_2. This also produces strongly anisotropic carrier effective masses, which are distinct for electrons and holes. The anisotropy of the band structure is an interesting feature of this class of compounds and should lead to anisotropic conductivity: we estimate a change of conductivity by a factor of 2-3 along two orthogonal directions (namely in the layer plane and out-of-plane) and in opposite directions for electrons and holes. Improved understanding of how these large effective masses manifest themselves in optical and electrical properties is key to the rational design of electronic and optical components based on $SnSe_{2(1-x)}S_{2x}$ for future applications.

ACKNOWLEDGMENTS

This work was supported by the Engineering and Physical Sciences Research Council (grant numbers EP/M012700/1 and EP/N01085X/1); the University of Nottingham; The National Academy of Sciences of Ukraine; The Leverhulme Trust (RF-2017- 224); the European Union's Horizon 2020 research and innovation programme Graphene Flagship Core 3; and the Chinese Academy of Sciences. The work at Jilin University is supported by the National Natural Science Foundation of China (grant numbers 61722403 and 11674121), Jilin Province Science and Technology Development Program (grant number 20190201016JC), and Program for Jilin University Science and Technology Innovative Research Team. Calculations were performed in part at the high-performance computing centre of Jilin University.

[1] B. Palosz, S. Gierlotka, and F. Levy, Polytypism of $SnSe_2$ crystals grown by chemical transport: structures of six large-period polytypes of $SnSe_2$, Acta Cryst. C **41**, 1404 (1985).

[2] B. Palosz, W. Steurer, and H. Schulz, Refinement of SnS_2 Polytypes 2H, 4H and 18R, Acta Cryst. B **46**, 449 (1990).

[3] Y. Wu, W. Li, A. Faghaninia, Z. Chen, J. Li, X. Zhang, B. Gao, S. Lin, B. Zhou, A. Jain, and Y. Pei, Promising thermoelectric performance in van der Waals layered $SnSe_2$, Mater. Today Phys. **3**, 127 (2017).

[4] B. Sun, Z. Ma, C. He, and K. Wu, Anisotropic thermoelectric properties of layered compounds in SnX_2 (X = S, Se): a promising thermoelectric material, Phys. Chem. Chem. Phys. **17**, 29844 (2015).

[5] Y. Su, M. A. Ebrish, E. J. Olson, and S. J. Koester, $SnSe_2$ field-effect transistors with high drive current, Appl. Phys. Lett. **103**, 263104 (2013).

[6] M. Li, D. Esseni, G. Snider, D. Jena, and H. G. Xing, Two-dimensional heterojunction interlayer tunneling field effect transistors, IEEE J. Electron Devices Soc. **3**, 200 (2017).

[7] T. S. Pan, D. De, J. Manongdo, A. M. Guloy, V. G. Hadjiev, Y. Lin, and H. B. Peng, Field effect transistors with layered two-dimensional $SnS_{2-x}Se_x$ conduction channels: Effects of selenium substitution, Appl. Phys. Lett. **103**, 093108 (2013).

[8] C. Fan, Y. Li, F. Lu, H.-X. Deng, Z. Wei, and J. Li, Wavelength dependent UV-Vis photodetectors from SnS_2 flakes, RSC Adv. **6**, 422 (2016).

[9] X. Zhou, L. Gan, W. Tian, Q. Zhang, S. Jin, H. Li, Y. Bando, D. Golberg, and T. Zhai, Ultrathin $SnSe_2$ Flakes Grown by Chemical Vapor Deposition for High-Performance Photodetectors, Adv. Mater. **27**, 8035 (2015).

[10] X. Wang, Z. Liu, X.-G. Zhao, J. Lv, K. Biswas, and L. Zhang, Computational Design of Mixed-Valence Tin Sulfides as Solar Absorbers, ACS Appl. Mater. Interfaces **11**, 24867 (2019).

[11] E. P. Mukhokosi, S. B. Krupanidhi, and K. K. Nanda, Band Gap Engineering of Hexagonal $SnSe_2$ Nanostructured Thin Films for Infra-Red Photodetection, Sci. Rep. **7**, 15215 (2017).

[12] E. Barrios-Salgado, M. T. S. Nair, and P. K. Nair, Thin films of n-type $SnSe_2$ produced from chemically deposited p-type SnSe, Thin Solid Films **598**, 149 (2016).

[13] C. Julien, M. Eddrief, I. Samaras, and M. Balkanski, Optical and electrical characterizations of SnSe, SnS_2 and $SnSe_2$ single crystals, Mater. Sci. Eng. B **15**, 70 (1992).

[14] Y. Huang, E. Sutter, J. T. Sadowski, M. Cotlet, O. L. A. Monti, D. A. Racke, M. R. Neupane, D. Wickramaratne, R. K. Lake, B. A. Parkinson, and P. Sutter, Tin Disulfide—An Emerging Layered Metal Dichalcogenide Semiconductor: Materials Properties and Device Characteristics, ACS Nano **8**, 10743 (2014).

[15] Y. W. Park, S.-K. Jerng, J. H. Jeon, S. B. Roy, K. Akbar, J. Kim, Y. Sim, M.-J. Seong, J. H. Kim, Z. Lee, M. Kim, Y. Yi, J. Kim, D. Y. Noh, and S.-H. Chun, Molecular beam epitaxy of large-area $SnSe_2$ with monolayer thickness fluctuation, 2D Mater. **4**, 014006 (2016).

[16] C. Guo, Z. Tian, Y. Xiao, Q. Mi, and J. Xue, Field-effect transistors of high-mobility few-layer $SnSe_2$, Appl. Phys. Lett. **109**, 203104 (2016).

[17] J. Singh, *Electronic and optoelectronic properties of semiconductor structures* (Cambridge Univ. Press, Cambridge, 2007).

[18] E. B. Lochocki, S. Vishwanath, X. Liu, M. Dobrowolska, J. Furdyna, H. G. Xing, and K. M. Shen, Electronic structure of $SnSe_2$ films grown by molecular beam epitaxy, Appl. Phys. Lett. **114**, 091602 (2019).

[19] F. A. Rasmussen and K. S. Thygesen, Computational 2D Materials Database: Electronic Structure of Transition-Metal Dichalcogenides and Oxides, J. Phys. Chem. C **119**, 13169 (2015).

[20] J. M. Gonzalez and I. I. Oleynik, Layer-dependent properties of SnS_2 and $SnSe_2$ two-dimensional materials, Phys. Rev. B **94**, 125443 (2016).

[21] A. Shafique, A. Samad, and Y.-H. Shin, Ultra low lattice thermal conductivity and high carrier mobility of monolayer SnS_2 and $SnSe_2$: a first principles study, Phys. Chem. Chem. Phys. **19**, 20677 (2017).

[22] Z. R. Kudrynskyi, X. Wang, J. Sutcliffe, M. A. Bhuiyan, Y. Fu, Z. Yang, O. Makarovsky, L. Eaves, A. Solomon, V. T. Maslyuk, Z. D. Kovalyuk, L. Zhang, and A. Patanè, Van der Waals $SnSe_{2(1-x)}S_{2x}$ Alloys: Composition-Dependent Bowing Coefficient and Electron–Phonon Interaction, Adv. Funct. Mater. **30**, 1908092 (2020).

[23] N. Miura, *Physics of semiconductors in high magnetic fields*, Vol. 15 (Oxford Univ. Press, Oxford, 2008).

[24] G. Kresse and J. Furthmüller, Efficient iterative schemes for ab initio total-energy calculations using a plane-wave basis set, Phys. Rev. B **54**, 11169 (1996).

[25] G. Kresse and J. Furthmüller, Efficiency of ab-initio total energy calculations for metals and semiconductors using a plane-wave basis set, Comput. Mater. Sci. **6**, 15 (1996).

[26] J. P. Perdew, K. Burke, and M. Ernzerhof, Generalized Gradient Approximation Made Simple, Phys. Rev. Lett. **77**, 3865 (1996).

[27] S. Grimme, Semiempirical GGA-type density functional constructed with a long-range dispersion correction, J. Comput. Chem. **27**, 1787 (2006).

[28] I. Hamada, Van der Waals density functional made accurate, Phys. Rev. B **89**, 121103 (2014).

[29] J. Klimes, D. R. Bowler, and A. Michaelides, Van der Waals density functionals applied to solids, Phys. Rev. B **83**, 195131 (2011).

[30] X. Wang, Y. Li, Y.-X. Pang, Y. Sun, X.-G. Zhao, J.-R. Wang, and L. Zhang, Rational design of new phases of tin monosulfide by first-principles structure searches, Sci. China Phys. Mech. **61**, 107311 (2018).

[31] A. V. Krukau, O. A. Vydrov, A. F. Izmaylov, and G. E. Scuseria, Influence of the exchange screening parameter on the performance of screened hybrid functionals, J. Chem. Phys. **125**, 224106 (2006).

[32] G. K. H. Madsen and D. J. Singh, BoltzTraP. A code for calculating band-structure dependent quantities, Comput. Phys. Commun. **175**, 67 (2006).

[33] X. Wang, D. Vanderbilt, J. R. Yates, and I. Souza, Fermi-surface calculation of the anomalous Hall conductivity, Phys. Rev. B **76**, 195109 (2007).

[34] M. Kawamura, FermiSurfer: Fermi-surface viewer providing multiple representation schemes, Comput. Phys. Commun. **239**, 197 (2019).

[35] See Supplemental Material at [URL will be inserted by publisher] for the layer thickness estimation, magneto-transmission on other samples, estimate of the energy uncertainty and conductivity effective mass.

[36] B. Evans and R. Hazelwood, Optical and electrical properties of $SnSe_2$, J. Phys. D Appl. Phys. **2**, 1507 (1969).

[37] N. Peyghambarian, S. W. Koch, and A. Mysyrowicz, *Introduction to semiconductor optics* (Prentice-Hall, Inc., 1993).

[38] A. Lipson, S. G. Lipson, and H. Lipson, *Optical physics* (Cambridge University Press, 2010).

[39] E. Rusu, N. Syrbu, A. Tiron, and V. Zalamai, Band structure and optical constants of SnS_2 single crystals, Mater. Res. Express **6**, 046203 (2019).

[40] J. J. Fox, X. Zhang, Z. Y. Al Balushi, M. Chubarov, A. Kozhakhmetov, and J. M. Redwing, Van der Waals epitaxy and composition control of layered SnS_xSe_{2-x} alloy thin films, J. Mater. Res. **35**, 1386 (2020).

[41] E. Kress-Rogers, R. J. Nicholas, J. C. Portal, and A. Chevy, Cyclotron resonance studies on bulk and two-dimensional conduction electrons in InSe, Solid State Commun. **44**, 379 (1982).

[42] J. Camassel, P. Merle, H. Mathieu, and A. Chevy, Excitonic absorption edge of indium selenide, Phys. Rev. B **17**, 4718 (1978).

[43] M. Millot, S. Gilliland, J. M. Broto, J. Gonzalez, J. Leotin, A. Chevy, and A. Segura, High pressure and high magnetic field behaviour of free and donor-bound-exciton photoluminescence in InSe, Phys. Status Solidi B **246**, 532 (2009).

[44] M. Millot, J.-M. Broto, S. George, J. González, and A. Segura, Electronic structure of indium selenide probed by magnetoabsorption spectroscopy under high pressure, Phys. Rev. B **81**, 205211 (2010).

[45] G. W. Mudd, M. R. Molas, X. Chen, V. Zólyomi, K. Nogajewski, Z. R. Kudrynskyi, Z. D. Kovalyuk, G. Yusa, O. Makarovsky, L. Eaves, M. Potemski, V. I. Fal'ko, and A. Patanè, The direct-to-indirect band gap crossover in two-dimensional van der Waals Indium Selenide crystals, Sci. Rep. **6**, 39619 (2016).

[46] S. Sasaki and N. Miura, New features in magneto-optical spectra of gaas/alxga1- xas short-period superlattices observed under pulsed high magnetic fields up to 150 t, Physica B Condens. Matter **184**, 111 (1993).

[47] K. Watanabe, K. Uchida, and N. Miura, Magneto-optical effects observed for gase in megagauss magnetic fields, Phys. Rev. B **68**, 155312 (2003).

[48] M. Dyksik, H. Duim, X. Zhu, Z. Yang, M. Gen, Y. Kohama, S. Adjokatse, D. K. Maude, M. A. Loi, D. A. Egger, *et al.*, Broad tunability of carrier effective masses in two-dimensional halide perovskites, ACS Energy Lett. **5**, 3609 (2020).

[49] J. Halpern and B. Lax, Magnetoabsorption of the indirect transition in germanium, J. Phys. Chem. Solids **26**, 911 (1965).

[50] L. M. Roth, B. Lax, and S. Zwerdling, Theory of Optical Magneto-Absorption Effects in Semiconductors, Phys. Rev. **114**, 90 (1959).

[51] M. Parish and P. Littlewood, Non-saturating magnetoresistance in heavily disordered semiconductors, Nature **426**, 162 (2003).

[52] N. Kozlova, N. Mori, O. Makarovsky, L. Eaves, Q. Zhuang, A. Krier, and A. Patanè, Linear magnetoresistance due to multiple-electron scattering by low-mobility islands in an inhomogeneous conductor, Nat. Commun. **3**, 1 (2012).

[53] B. Bansal, M. Hayne, B. Arora, and V. V. Moshchalkov, Magnetic field-dependent photoluminescence linewidths as a probe of disorder length scales in quantum wells, Appl. Phys. Lett. **91**, 251108 (2007).

[54] T. Jia, Z. Feng, S. Guo, X. Zhang, and Y. Zhang, Screening Promising Thermoelectric Materials in Binary Chalcogenides through High-Throughput Computations, ACS Appl. Mater. Interfaces **12**, 11852 (2020).

[55] W. Nakwaski, Effective masses of electrons and heavy holes in GaAs, InAs, A1As and their ternary compounds, Physica B: Condens. Matter. **210**, 1 (1995).

[56] Z. Yang, A. Surrente, K. Galkowski, A. Miyata, O. Portugall, R. J. Sutton, A. A. Haghighirad, H. J. Snaith, D. K. Maude, P. Plochocka, and R. J. Nicholas, Impact of the Halide Cage on the Electronic Properties of Fully Inorganic Cesium Lead Halide Perovskites, ACS Energy Lett. **2**, 1621 (2017).

[57] K. Galkowski, A. Mitioglu, A. Miyata, P. Plochocka, O. Portugall, G. E. Eperon, J. T.-W. Wang, T. Stergiopoulos, S. D. Stranks, H. J. Snaith, and R. J. Nicholas, Determination of the exciton binding energy and effective masses for methylammonium and formamidinium lead tri-halide perovskite semiconductors, Energy Environ. Sci. **9**, 962 (2016).

[58] A. M. Soufiani, Z. Yang, T. Young, A. Miyata, A. Surrente, A. Pascoe, K. Galkowski, M. Abdi-Jalebi, R. Brenes, J. Urban, *et al.*, Impact of microstructure on the electron–hole interaction in lead halide perovskites, Energy Environ. Sci. **10**, 1358 (2017).

[59] Z. Yang, A. Surrente, K. Galkowski, N. Bruyant, D. K. Maude, A. A. Haghighirad, H. J. Snaith, P. Plochocka, and R. J. Nicholas, Unraveling the exciton binding energy and the dielectric constant in single-crystal methylammonium lead triiodide perovskite, J Phys. Chem. Lett. **8**, 1851 (2017).

[60] A. R. Beal and W. Y. Liang, Excitons in 2H-WSe_2 and 3R-WS_2, J. Phys. C **9**, 2459 (1976).

[61] A. Stier, N. Wilson, K. Velizhanin, J. Kono, X. Xu, and S. Crooker, Magnetooptics of Exciton Rydberg States in a Monolayer Semiconductor, Phys. Rev. Lett. **120**, 057405 (2018).

[62] Z. Wang, C. Fan, Z. Shen, C. Hua, Q. Hu, F. Sheng, Y. Lu, H. Fang, Z. Qiu, and J. Lu, Defects controlled hole doping and multivalley transport in SnSe single crystals, Nat. Commun. **9**, 1 (2018).

[63] D. A. Bandurin, A. V. Tyurnina, G. L. Yu, A. Mishchenko, V. Zólyomi, S. V. Morozov, R. K. Kumar, R. V. Gorbachev, Z. R. Kudrynskyi, S. Pezzini, Z. D. Kovalyuk, U. Zeitler, K. S. Novoselov, A. Patanè, L. Eaves, I. V. Grigorieva, V. I. Fal'ko, A. K. Geim, and Y. Cao, High electron mobility, quantum Hall effect and anomalous optical response in atomically thin InSe, Nat. Nanotechnol. **12**, 223 (2017).

[64] T. M. Brenner, D. A. Egger, A. M. Rappe, L. Kronik, G. Hodes, and D. Cahen, Are Mobilities in Hybrid Organic–Inorganic Halide Perovskites Actually "High"?, J Phys. Chem. Lett. **6**, 4754 (2015).

[65] G. Dresselhaus, A. F. Kip, and C. Kittel, Cyclotron Resonance of Electrons and Holes in Silicon and Germanium Crystals, Phys. Rev. **98**, 368 (1955).